

UPPER LIMITS ON THE MASSES OF 105 SUPERMASSIVE BLACK HOLES FROM HST/STIS ARCHIVAL DATA¹A. BEIFIORI², M. SARZI³, E. M. CORSINI², E. DALLA BONTÀ², A. PIZZELLA², L. COCCATO⁴, AND F. BERTOLA²*Draft version August 31, 2018*

ABSTRACT

Based on the modeling of the central emission-line width measured over sub-arcsecond apertures with the *Hubble Space Telescope*, we present stringent upper bounds on the mass of the central supermassive black hole, M_{\bullet} , for a sample of 105 nearby galaxies ($D < 100$ Mpc) spanning a wide range of Hubble types (E – Sc) and values of the central stellar velocity dispersion, σ_c (58 – 419 km s⁻¹). For the vast majority of the objects the derived M_{\bullet} upper limits run parallel and above the well-known $M_{\bullet} - \sigma_c$ relation independently of the galaxy distance, suggesting that our nebular line-width measurements trace rather well the nuclear gravitational potential. For values of σ_c between 90 and 220 km s⁻¹ the 68% of our upper limits falls immediately above the $M_{\bullet} - \sigma_c$ relation without exceeding the expected M_{\bullet} values by more than a factor 4.1. No systematic trends or offsets are observed in this σ_c range as a function of the galaxy Hubble type or with respect to the presence of a bar. For 6 of our 12 M_{\bullet} upper limits with $\sigma_c < 90$ km s⁻¹ our line-width measurements are more sensitive to the stellar contribution to the gravitational potential, either due to the presence of a nuclear stellar cluster or because of a greater distance compared to the other galaxies at the low- σ_c end of the $M_{\bullet} - \sigma_c$ relation. Conversely, our M_{\bullet} upper bounds appear to lie closer to the expected M_{\bullet} in the most massive elliptical galaxies with values of σ_c above 220 km s⁻¹. Such a flattening of the $M_{\bullet} - \sigma_c$ relation at its high- σ_c end would appear consistent with a coevolution of supermassive black holes and galaxies driven by dry mergers, although better and more consistent measurements for σ_c and K -band luminosity are needed for these kind of objects before systematic effects can be ruled out.

Subject headings: black hole physics, galaxies: kinematics and dynamics, galaxies: structure

1. INTRODUCTION

Supermassive black holes (SMBHs) have now been discovered in the center of a sufficiently large number of nearby galaxies to probe possible links between the masses of SMBHs (M_{\bullet}) and the global properties of their host galaxies. In fact, it has emerged that M_{\bullet} correlates with the luminosity (Kormendy & Richstone 1995; Marconi & Hunt 2003), mass (Magorrian et al. 1998; Häring & Rix 2004), stellar velocity dispersion (Ferrarese & Merritt 2000; Gebhardt et al. 2000; Tremaine et al. 2002; Ferrarese & Ford 2005), light concentration (Graham et al. 2001), and gravitational binding energy (Aller & Richstone 2007) of the host-galaxy spheroidal component, i.e., the entire galaxy in the case of elliptical galaxies or the bulge of disk galaxies. In light of these findings it is now widely accepted that the mass-accretion history of a SMBH is tightly related through feedback to the formation and evolution of the host

spheroid (e.g., Silk & Rees 1998; Haehnelt & Kauffmann 2000; Di Matteo et al. 2005), some studies having suggested a link with the mass of the dark-matter halo (Ferrarese 2002; Pizzella et al. 2005).

The slope and scatter of all these correlations remain quite uncertain (Novak et al. 2006), however, in particular since they are still based on a limited sample of galaxies with reliable M_{\bullet} that is biased towards early-type systems and that is clustered around a rather limited range of stellar velocity dispersion (σ), approximately between 150 and 250 km s⁻¹. Given the great theoretical interest spurred by these findings, there is a pressing need to acquire better M_{\bullet} statistics, both in terms of the number of targets and in terms of broadening the range of parent galaxies, in particular towards spiral galaxies.

Secure M_{\bullet} measurements in external galaxies are traditionally obtained through the modeling of the stellar and/or gaseous kinematics, most often as derived using *Hubble Space Telescope* (*HST*) observations in the optical domain. The advent of adaptive-optics systems working at near-infrared wavelengths has led to

¹ Based on observations with the NASA/ESA *Hubble Space Telescope* obtained at STScI, which is operated by the Associ-

Cappellari & McDermid 2005). Water-masers have provided the most accurate extragalactic M_{\bullet} measurements to date, but such gaseous systems are exceedingly rare (Braatz et al. 1994; Greenhill et al. 2003). The modeling of the nuclear ionized-gas kinematics has also led to accurate M_{\bullet} measurements (e.g., Barth et al. 2001; Dalla Bontà et al. 2008), and at a relatively cheap cost in terms of observation time compared to stellar-dynamical M_{\bullet} determinations (e.g., Verolme et al. 2002; Gebhardt et al. 2003). Yet, only a handful of the objects targeted by HST turned out to have sufficiently regular gas velocity fields for the purpose of modeling (Sarzi et al. 2001). Thus, unless a large number of galaxies pre-selected to have regular nuclear gas kinematics (for instance following Ho et al. 2002) is observed with HST if and when the Space Telescope Imaging Spectrograph (STIS) is successfully refurbished, it is unlikely that the number of galaxies with secure M_{\bullet} measurements will increase dramatically in the near future.

The HST Science Archive already contains an untapped resource that can be used to better constrain the black-hole mass budget across the different morphological types of galaxies, which consists of the vast number of the STIS spectra from which a central emission-line width can be measured. The modeling of this kind of data can indeed lead to tight upper limits on M_{\bullet} , as first shown by Sarzi et al. (2002). For this reason we started a program aimed at deriving M_{\bullet} upper limits based on HST spectra for the largest possible number of galaxies and a wide range of morphological types. In this paper we present the results based on a sample of 105 nearby galaxies for which STIS/G750M spectra in the H α region and measurements of the stellar velocity dispersion were available from the HST archive and in the literature, respectively. Although we will be able only to set an upper limit on the M_{\bullet} of our galaxies, the lack of exact measurements will be compensated for by the large number of upper limits when studying SMBH mass-host galaxy relationships.

The paper is organized as follows. In § 2 we describe our sample selection and the measurement of central emission-line width, before briefly describing our modeling. We will then present our results and discuss our findings in the context of the $M_{\bullet} - \sigma$ relation between the SBHM mass and central stellar velocity dispersion of the host spheroid in § 3.

2. DATA COMPILATION AND ANALYSIS

2.1. Sample selection and data reduction

In order to assemble the largest possible sample of homogeneous measurements of the central emission-line width, we queried the HST Science Archive for objects

measurements based either on surface-brightness fluctuations (Tonry et al. 2000; Tonry et al. 2001), Cepheid variables (Freedman et al. 2001) or from Tully (1988). Otherwise we used the weighted mean recessional velocity corrected to the reference frame defined by the microwave background radiation from de Vaucouleurs et al. (1991, RC3 hereafter) to derive the distance to our sample galaxies by assuming $H_0 = 75 \text{ km s}^{-1} \text{ Mpc}^{-1}$, $\Omega_m = 0.3$, and $\Omega_{\Lambda} = 0.7$. The median distance of the sample galaxies is 21.4 Mpc.

The archival spectra were reduced using IRAF⁵ and the STIS reduction pipeline maintained by the Space Telescope Science Institute (Dressel et al. 2007). The basic reduction steps included overscan subtraction, bias subtraction, dark subtraction, and flatfield correction. Different spectra obtained for the same slit position were aligned using IMSHIFT and knowledge of the adopted shifts along the slit position. Cosmic ray events and hot pixels were removed using the task LACOS_SPEC by van Dokkum (2001). Residual bad pixels were corrected by means of a linear one-dimensional interpolation using the data quality files and stacking individual spectra with IMCOMBINE. This allowed to increase the signal-to-noise ratio of the resulting spectra. We performed wavelength and flux calibration as well as geometrical correction for two-dimensional distortion following the standard reduction pipeline and applying the X2D task. This task corrected the wavelength scale to the heliocentric frame too.

To measure the nuclear emission-line width we generally extracted aperture spectra three ($0''.15$) and five pixels wide ($0''.25$) centered on the continuum peak, for the $0''.1$ and $0''.2$ -wide slit cases, respectively. When the spectra were obtained with a 2-pixel binning read-out mode along the spatial direction, we extracted aperture spectra three pixels wide ($0''.3$) for the $0''.2$ -wide slit (Table 1). The extracted spectra thus consist of the central emission convolved with the STIS spatial point-spread function (PSF) and sampled over nearly square apertures of $0''.15 \times 0''.1$, $0''.25 \times 0''.2$ or $0''.3 \times 0''.2$, roughly corresponding to a circular aperture with a radius of $0''.07$, $0''.13$, and $0''.14$, respectively. The wavelength range of our spectra is either 6482–7054 Å or 6295 – 6867 Å, depending on whether the G750M grating was used at the primary or secondary tilt. The instrumental FWHM was 0.87 Å ($\sigma_{\text{inst}} = 17 \text{ km s}^{-1}$) and 1.6 Å ($\sigma_{\text{inst}} = 32 \text{ km s}^{-1}$) for the $0''.1$ and the $0''.2$ -wide slit, respectively. The atlas of all the extracted spectra will be presented in a forthcoming paper.

To place our M_{\bullet} upper limits with the $M_{\bullet} - \sigma$ relation, here we consider only galaxies with velocity dispersion measurements in the literature, which were available for 137 objects. We also dropped a further five objects, since

tions in the emission-line flux profiles across the nucleus. As constraining the concentration of the nebular emission is key to our modeling (see §2.3), this problem forced us to remove a further eight galaxies from our sample.

2.2. Measurement of the emission lines

In order to derive upper limits on M_{\bullet} following the method of Sarzi et al. (2002, see also §2.3) we need to measure both the width of the central nebular emission and the radial profile of the emission-line flux, so that we can gauge both the depth of the potential well and the concentration of its gaseous tracer. To side-step the impact of broad and/or asymmetric emission arising from regions much smaller than our resolution limit, we focus on the width of the narrow component of the emission from forbidden transitions and disregard the broad-line emission in our spectra. In the wavelength range of our spectra that means measuring the central width and flux profile of the [N II] $\lambda\lambda 6548, 6583$ lines since these are usually brighter than the [S II] $\lambda\lambda 6716, 6731$ lines. The [N II] doublet also traces the nuclear kinematics better than $H\alpha$, given that this line could be significantly affected by emission from circumnuclear star-forming regions (e.g., Verdoes Kleijn et al. 2000; Coccato et al. 2006).

To measure the central width and flux profile of the narrow component of the [N II] lines we fit our spectra with multiple Gaussians to match both the broad and narrow components of all the observed lines, while describing the stellar continuum with a low-order polynomial. A flux ratio of 1:3 was assumed for the [N II] doublet, as dictated by atomic physics (e.g., Osterbrock 1989), and in the presence also of [S II] emission, both the [N II] and [S II] doublets were assumed to share a common line centroid and width. In most cases only one additional Gaussian component was needed in our fits, to describe the $H\alpha$ emission from the broad-line region, although in many objects also the forbidden [N II] and [S II] lines required double-Gaussian profiles. This allowed us to describe also lines with Voigt profiles, where tests on 18 galaxies showed that our narrowest Gaussian component tend to be only slightly broader than the thermal component in the Voigt profiles, generally by less than 20%. The extra Gaussian in the [N II] and [S II] lines was also used to isolate the contribution of blue- or redshifted wings. To help deblending the $H\alpha + [N II]$ region in some cases we followed Ho et al. (1997) and assigned to both the [N II] lines and the narrow $H\alpha$ emission the line profile that was predetermined by fitting the [S II] lines. The best-fitting Gaussian parameters were derived using a non-linear least-squares minimization based on the robust Levenberg-Marquardt method (e.g., Press et al. 1996) implemented by Moré et al. (1980). The actual

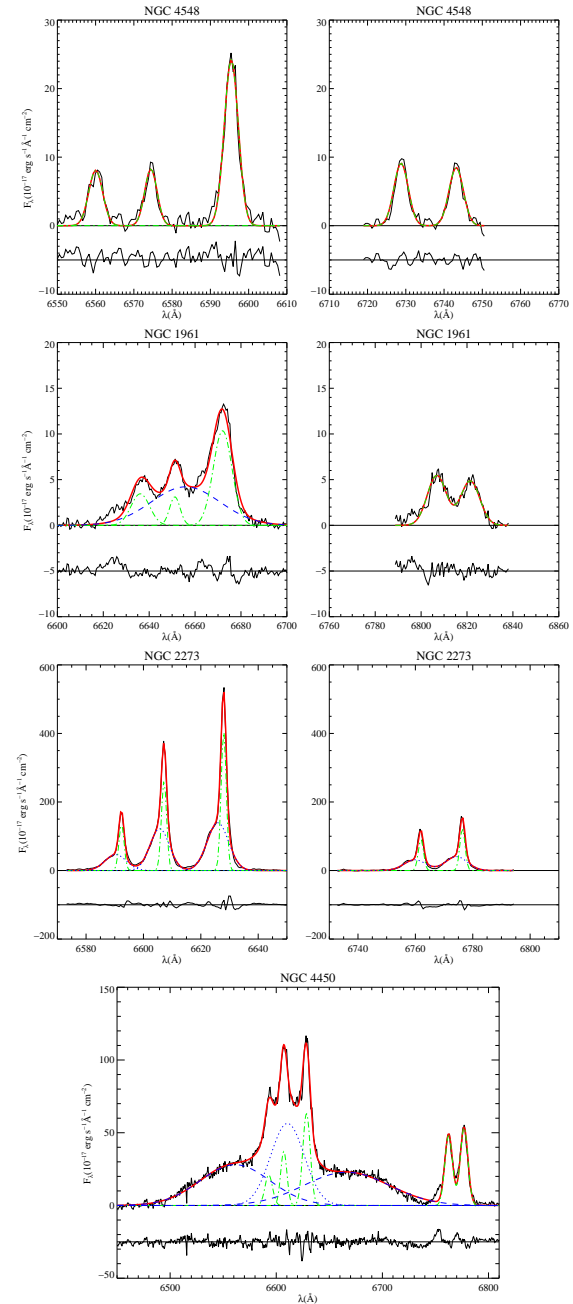


FIG. 1.— Few examples of continuum-subtracted central G750M spectra from our spectral atlas illustrating the various fitting strategies adopted to match $H\alpha$, [N II] $\lambda\lambda 6548, 6583$ and [S II] $\lambda\lambda 6716, 6731$ emission lines. In each panel the red line show the overall line blend, whereas the green dashed-dotted lines and blue dotted or dashed lines show the adopted narrow and broad Gaussian components, respectively. Shown are also the fit resid-

(300 Myr) or old (10 Gyr) stellar population templates. In most cases the measurements agreed within the errors, except for IC 342 and NGC 7331 where the H α absorption line is particularly prominent. For these galaxies we adopted the GANDALF values. Finally, in defining our detection thresholds we compared the amplitude (A) of the best-fitting line profile to the noise level (N) in the residuals of the continuum fit, adopting as detected only those emission lines for which the A/N ratio was larger than 3. Figure 1 shows a few sample spectra illustrating the various fitting strategies explained above. A more detailed description of our emission-line measurements for each of our sample galaxy will be presented with our spectral atlas.

In 14 galaxies the nebular emission was too faint for it to be detected given the quality of the corresponding spectra, and were consequently dropped from our sample. Three further galaxies had also to be discarded because their line profile could not be well represented as a simple sum of Gaussian components. Finally, two galaxies were rejected because the radial profile of the flux of the [N II] lines was strongly asymmetric and not suitable for modelling. Table 1 lists the final sample of galaxies analyzed in this paper, which comprises of 105 galaxies which 28 (27%) are classified as ellipticals, 20 (19%) are lenticulars, and 57 (54%) are spirals. The central velocity dispersion of the ionized-gas component and the size of the aperture we measured are also given in Table 1. Prior to modeling, the instrumental resolution corresponding to the adopted apertures (17 km s $^{-1}$ and 32 km s $^{-1}$ for the 0".1 and 0".2 slit widths, respectively) was subtracted in quadrature from the observed line-width values to obtain the intrinsic gas velocity dispersion.

Table 2 lists the 74 rejected galaxies.

2.3. Modeling the central line width

Assuming that the width of the nuclear emission traces the depth of the gravitational well, we can derive stringent upper bounds on the mass of the SMBHs in our sample galaxies thanks to the exquisite spatial resolution of HST. Although the stellar contribution to the gravitational potential could affect such estimates, the fundamental reason for which a lower limit on M_{\bullet} can not be set from such a simple measurements is that the observed line-broadening may, in principle, be entirely due to additional contributions such as non-gravitational forces (e.g., gas pressure or magnetic forces).

In this study we follow the procedure described in Sarzi et al. (2002), where a detailed description of the method can be found. In short, we assume that the observed line-broadening arises from the motion of ionized-gas in a coplanar thin inner disk of unknown inclination, where the gas moves in circular and Keplerian orbits

ply considering models with nearly edge-on ($i = 81^{\circ}$, $\cos i = 0.16$) and face-on ($i = 33^{\circ}$, $\cos i = 0.84$) orientations, respectively, comprising 68% of the distribution of M_{\bullet} values that can explain a given line width (e.g., Sarzi et al. 2002).

In our models we could disregard the effect on the unknown position angle of the disk since we extracted our spectra in nearly square apertures, and thus assumed that the STIS slit was placed along the disk major axis.

Clearly, for a given disk orientation the concentration of the gas tracer impacts heavily on the M_{\bullet} value needed to explain a given line width, to the point that no lower limit on M_{\bullet} can be set when the gas profile is unresolved. This is why the intrinsic emissivity distribution of the gaseous disk has to be constrained from the data. As in Sarzi et al. (2002), we assumed an intrinsically Gaussian flux profile centered on the stellar nucleus, which makes it easier to match the observed flux profile while accounting for instrumental effects. The choice of a Gaussian parametrization is also conservative, since cuspier functions would have led us to estimate smaller M_{\bullet} . For instance, adopting an exponential profile for the subsample of objects studied also by Sarzi et al. (2002) leads on average to a 10% decrease for the M_{\bullet} estimates.

In this work we disregarded the contribution of the stellar potential, which would lead to tighter upper limits on M_{\bullet} . In principle, it is possible to estimate the stellar mass contribution by deprojecting the stellar surface brightness observed in the STIS acquisition images while assuming spherical symmetry and a constant mass-to-light ratio (Sarzi et al. 2002). In practice, however, this would only be feasible for a limited number of objects in our sample, given the limited quality of the acquisition images for most of our sample galaxies, and the pervasive presence of dust absorption features, in particular in spiral host galaxies. Still, the impact of the stellar potential is unlikely to change dramatically our M_{\bullet} estimates, in particular for the upper limits derived for nearly face-on configurations. For their sample of nearby galaxies (at 8 – 17 Mpc), Sarzi et al. (2002) found that including the stellar mass contribution reduced the median value of the M_{\bullet} upper limits by just $\sim 12\%$. For the median distance our sample (21.4 Mpc) the stellar mass contribution to our 33° upper-limits would be $\sim 15\%$. Similar considerations would apply to the M_{\bullet} sensitivity limit of our experiment. In the case of the Sarzi et al. (2002) sample this value was found to be on average $3.9 \times 10^6 M_{\odot}$, which is well below most of the M_{\bullet} limits derived here and comparable to the smallest M_{\bullet} limits obtained for the closest objects in our sample.

To conclude, we note that the range spanned by the two M_{\bullet} values delivered by our Keplerian-disk model includes also M_{\bullet} that would be estimated under radically

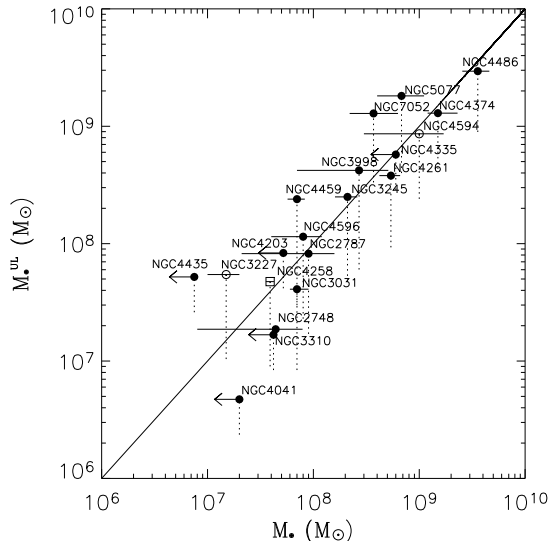


FIG. 2.— Comparison between our M_{\bullet} upper limits and accurate measurements of M_{\bullet} based on the resolved kinematics of gas (filled circles), stars (open circles), and water masers (open square) available in the literature. Leftward arrows indicate an upper constrain rather than a definite value for M_{\bullet} . The upper and lower edges of the dotted lines correspond to the M_{\bullet} values that we estimated assuming an inclination of $i = 33^{\circ}$ and 81° for the unresolved Keplerian disk, respectively.

We have determined the 1σ upper and lower confidence limits for the M_{\bullet} for randomly orientated disks for 105 galaxies with measurable spectra and stellar velocity dispersions available in the literature. For 19 galaxies of the sample, either M_{\bullet} measurements or upper limits based on resolved kinematics were available (Table 1). Fig. 2 shows how such measurements compare with our M_{\bullet} limits, once our values are rescaled accordingly to the distances adopted in these studies. Our M_{\bullet} upper-limits are consistent within 1σ with such estimates, except for NGC 3031 and NGC 4261. Furthermore no systematic offset appears when our upper limits are compared with similar upper bounds in the literature, rather than definite measurements. A particularly complex blend of narrow $H\alpha$ + $[N\text{II}]$ and broad $H\alpha$ lines may have biased our M_{\bullet} estimates in NGC 3031.

To place our M_{\bullet} limits on the various versions of the $M_{\bullet} - \sigma$ relation, we applied to the aperture correction of Jørgensen et al. (1995) to the literature values of stellar velocity dispersion in order to obtain the values σ_c and σ_e and that would have been measured within a circular aperture of radius $r_e/8$ and r_e , respectively. The effective radii r_e of the spheroidal components of our sample galaxies were taken from various sources in the literature (Table 1) except for few disk galaxies for which r_e was

rank coefficient of 0.9 suggests the presence of a correlation at 9σ confidence level whereas a Pearson correlation coefficient of 0.8 supports a linear fit to the logarithmic data, which returns a slope of 3.43 ± 0.21 . At first glance such a value would imply a shallower trend than found by Ferrarese & Ford (2005) and a slope closer to that of the Lauer et al. (2007) relation, but we need to keep in mind that the derived slope could be significantly affected by just a few outliers. In particular, for small value of σ our M_{\bullet} upper-limits could be biased owing to a larger stellar contribution to the gravitational potential in small and distant galaxies. On the other hand, we found that our limits appear to parallel particularly well both versions of the $M_{\bullet} - \sigma$ relation for $90 \leq \sigma_c, \sigma_e \leq 220 \text{ km s}^{-1}$, whereas at lower and higher σ a substantial fraction of our M_{\bullet} limits lie either considerably above or almost on top of the $M_{\bullet} - \sigma$ relation, respectively.

In the following sections we better quantify and interpret these first considerations.

3.1. Main trend in the sample

In the σ_c interval between 90 and 220 km s^{-1} our M_{\bullet} upper limits appear to correlate particularly well with σ_c , paralleling the $M_{\bullet} - \sigma_c$ relation. In this σ_c region a value of 0.8 for the Spearman’s rank correlation coefficient suggests the presence of a correlation at a $7\text{-}\sigma$ confidence level, whereas a Pearson coefficient of 0.8 indicates that the logarithm values of our M_{\bullet} upper limits and σ_c are very likely to be linearly correlated. A linear fit in the $\log \sigma_c - \log M_{\bullet}$ plane delivers a best-fitting slope of 4.52 ± 0.41 for our M_{\bullet} upper limits, compared to the 4.86 ± 0.43 slope of the Ferrarese & Ford (2005) relation, with a scatter of 0.39 dex (Figs. 5a). In the $90 \leq \sigma_c \leq 220 \text{ km s}^{-1}$ interval we have 66 M_{\bullet} upper limits, which have a median 2.7 times higher than the expected M_{\bullet} value (Fig. 5c). These upper-limits can range from falling short of the expected M_{\bullet} values by a factor 3.7 to exceeding them by a factor 17.3, although 68% of them actually do not top the expected M_{\bullet} values by more than a factor 4.1 and fall immediately above the $M_{\bullet} - \sigma_c$ relation. For comparison, by fitting our upper limits in the $M_{\bullet} - \sigma_e$ plane we obtain a slope of 4.12 ± 0.38 , very close to the value of 4.13 ± 0.32 found by Lauer et al. (2007). In fact, the parallel trend of our upper limits holds as far as $\sigma_e \sim 300 \text{ km s}^{-1}$, with a Spearman’s rank coefficient of 0.8, a Pearson linear correlation coefficient of 0.8 and a linear slope of 3.84 ± 0.28 .

Fig. 3a shows that such a trend holds independent of galactic distance – objects as far away as 60 Mpc appear to run parallel to the $M_{\bullet} - \sigma_c$ relation. In particular, the objects at and below 20 Mpc are well distributed. In fact, if in this range of σ_c we perform separate linear regression

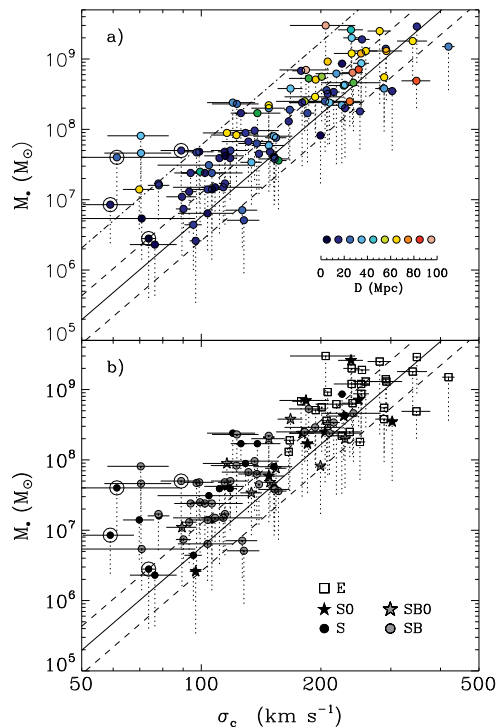


FIG. 3.— Comparison between our M_{\bullet} upper limits and $M_{\bullet} - \sigma_c$ relation by Ferrarese & Ford (2005) (thick line) as a function of galaxy distance (a) and morphological type (b). The upper and lower edges of the dotted lines correspond to M_{\bullet} values estimated assuming an inclination of $i = 33^\circ$ and 81° for the unresolved Keplerian disk, respectively. Large circles mark galaxies with $\sigma_c < 90 \text{ km s}^{-1}$ that host a nuclear star cluster. The dashed lines show to the 1σ (0.34 dex) scatter in M_{\bullet} . Additionally, to follow the discussion in §3.1 and §3.2, the dot-dashed line shows the 3σ (1.02 dex) scatter above the $M_{\bullet} - \sigma$ relation whereas the open circles point to objects where a nuclear cluster is present.

arises predominantly in regions of the gravitational potential that are dominated by the influence of the central SMBHs.

This is not completely unexpected given that a number of HST observations revealed that the narrow-line regions of active nuclei appear to be quite concentrated with scales less than 50 pc, much more so than the underlying stellar density profile (see, e.g., Ho 2008). Most recently, Walsh et al. (2008) have mapped the behavior of the narrow-line region for galaxies observed with multiple-slit STIS observations. They found that all galaxies of their sample exhibit a centrally peaked surface-brightness profile, with the majority of them further showing a marked gradient of the emission-line widths within the sphere of influence of the central SMBH. The high degree of concentration of the gaseous

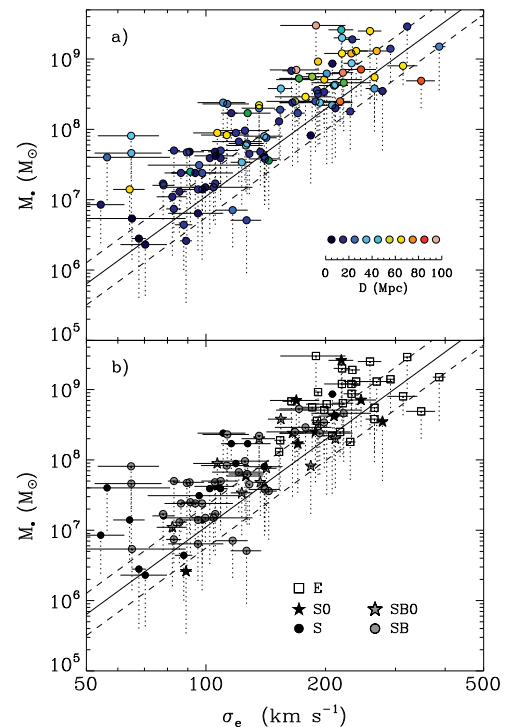


FIG. 4.— Same as Fig. 3 but now showing the comparison between our M_{\bullet} upper limits and the $M_{\bullet} - \sigma_e$ relation of Lauer et al. (2007)

the observed line widths (unless for some reason their importance scales with σ_c), although their role cannot be firmly excluded on a single-case basis.

Fig. 3b also shows that in the $\sigma_c = 90 - 220 \text{ km s}^{-1}$ range the upper limits derived in galaxies of different Hubble types lie neither closer nor further away from the $M_{\bullet} - \sigma_c$ relation, although only a relatively small number of elliptical galaxies falls in this σ_c interval. Similarly, even though only 38% of the spiral and lenticular galaxies in this σ_c region are unbarred we do not notice any systematic trend with the presence of a bar, unlike what was found by Graham (2008).

Since our upper limits appear to trace quite closely the expected values for M_{\bullet} , we can take advantage of the significant number of galaxies in our sample to understand whether the objects that within the present σ_c range appear to show remarkably large or small upper-bounds are in fact exceptional. Assuming that our 1σ limits bracket symmetrically the expected values of M_{\bullet} and that our upper bounds lie 2.7 times above the $M_{\bullet} - \sigma_c$ relation, with the aid of a Monte Carlo simulation we found that 16% of our M_{\bullet} upper limits should lie above the $M_{\bullet} - \sigma_c$

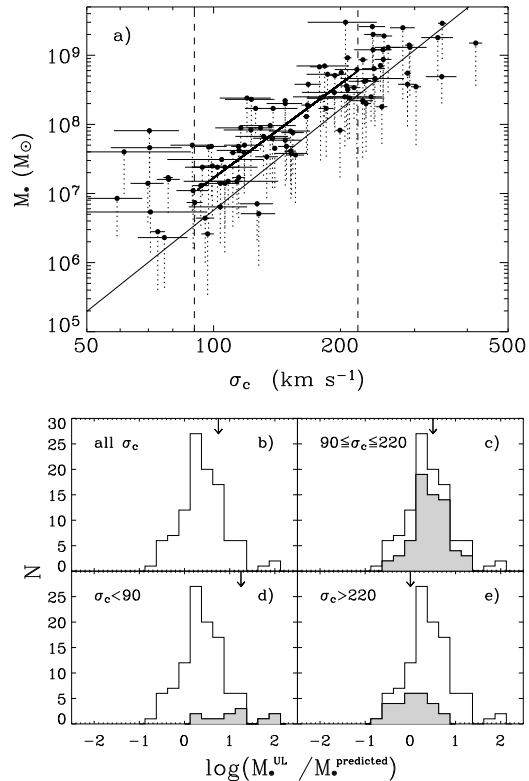


FIG. 5.— *Upper panel (a)*: Comparison between the linear fit to the M_{\bullet} upper limits in the range $90 \leq \sigma_c \leq 220 \text{ km s}^{-1}$ (thick line) and the $M_{\bullet} - \sigma_c$ relation by Ferrarese & Ford (2005, thin line). Our linear fit to the M_{\bullet} upper limits in the $90 \leq \sigma_c \leq 220 \text{ km s}^{-1}$ range (shown by the vertical dashed lines) delivers a best-fitting slope of 4.52 ± 0.41 . *Lower panels*: Distribution of the ratios between the measured upper limits and the values of M_{\bullet} expected from the $M_{\bullet} - \sigma_c$ relation by Ferrarese & Ford (2005) for (b) all the sample galaxies, (c) the galaxies with $90 \leq \sigma_c \leq 220 \text{ km s}^{-1}$, (d) with $\sigma_c < 90 \text{ km s}^{-1}$, and (e) with $\sigma_c > 220 \text{ km s}^{-1}$. The median of each distribution is marked by an arrow.

tic nuclei, and further suggests that galaxies with considerably smaller M_{\bullet} -budgets (i.e., below the $M_{\bullet} - \sigma_c$ relation by more than its scatter) may be particularly rare. The presence of undermassive SMBHs in field galaxies have been suggested for instance by Vittorini et al. (2005), who argued that in a low galactic-density environment the M_{\bullet} growth may be hampered by the lack of gaseous fuel. A population of undermassive SMBH was discovered also by Volonteri (2007) in her simulations of the last stages of black-hole mergers, when the binary experiences a recoil due to asymmetric emission of gravitational radiation. According to Fig. 4 of Volonteri (2007) up to 25% of the galaxies with $90 \leq \sigma_c \leq 220 \text{ km s}^{-1}$

low-end of the luminosity function where most galaxies are found. Our constraints should therefore be regarded with caution.

3.2. The lower end of the $M_{\bullet} - \sigma_c$ relation

At small σ_c ($< 90 \text{ km s}^{-1}$) half of our upper limits systematically exceed the expected M_{\bullet} values by 3 times the scatter of the $M_{\bullet} - \sigma_c$ relation. They are in average larger by more than a factor 40 (Fig. 5d), consistent with previous works on much more smaller samples (Sarzi et al. 2002; Sarzi 2004; Verdoes Kleijn et al. 2006). They are hosted by NGC 3021, NGC 4245, NGC 5347, NGC 5427, NGC 5879, and UGC 1395, which are late-type spirals with different degrees of nuclear activity, as measured by Ho, Filippenko, & Sargent (1997, see Table 1).

We have considered different possibilities related to the measurement and modeling of the $[\text{N II}] \lambda 6583$ emission line to explain the high values of M_{\bullet} found in these 6 objects. For instance, the presence of broad or asymmetric components in our spectra could affect the width of the narrow component of the $[\text{N II}]$ lines that we measured and consequently the M_{\bullet} upper limits giving larger masses. A similar bias would be introduced if the extent of the flux profile were to be systematically overestimated. Blue asymmetries are observed in the top outliers NGC 5347 and NGC 5427, which are also part of the sample of active galactic nuclei studied by Rice et al. (2006), who investigated the resolved kinematics of their narrow-line region with STIS spectra and first reported the presence of blue wings in the $[\text{S II}] \lambda \lambda 6716, 6731$ lines. In our fits, however, the contribution of such additional features was isolated using double Gaussian profiles. As regards the flux profile of the $[\text{N II}]$ doublet of the small- σ_c outliers, these are not systematically shallower than the other galaxies following the $M_{\bullet} - \sigma_c$ relation in the same σ_c range. Therefore, the M_{\bullet} upper limits that we have calculated are not biased by either of these effects.

To explain the largest M_{\bullet} upper limits found at low σ_c values we also considered the impact of the presence of a nuclear star cluster (NC), and in general that of a larger stellar contribution due to a greater distance. NCs are massive stellar clusters coincident with the galaxy photo-center (Côté et al. 2006) that are found in about 75% of late-type spiral galaxies (Böker et al. 2002). Their mean effective radius is $\sim 3.5 \text{ pc}$ (Böker et al. 2004), small enough for them to be completely enclosed within the central aperture of our spectra. Ferrarese et al. (2006) found a different $M_{\bullet} - \sigma_c$ relation for NCs, with similar slope but a normalization that is larger by roughly an order of magnitude than that the one found for SMBHs. The presence of NCs in our low- σ_c outliers could therefore explain why they show such high central mass con-

the low- σ_c end of our sample is shown in Fig. 3, and in the case of NGC 3021 and NGC 5879 it was already known (see Scarlata et al. 2004; Seth et al. 2008, respectively). If our limits trace indeed the dynamical signature of a NC in these nuclei, better data and more detailed modelling (e.g., Barth et al. 2008) would be required to disentangle the contribution of the NC and SMBH to the total mass budget. As regards the distance of the low- σ_c outliers, although we can only rely on distances inferred from their recessional velocities it is significant that half of them (NGC 5347, NGC 5427, and UGC 1395) are found beyond 30 Mpc, whereas all the other low- σ_c galaxies are significantly closer, including those for which our M_\bullet upper limits lie well within 3 times the scatter of $M_\bullet - \sigma_c$ relation.

These findings suggest that part, if not all, of the exceedingly large M_\bullet values we found at the low- σ_c end of the $M_\bullet - \sigma_c$ relation could be ascribed to a more significant stellar contribution to the gravitational potential. This is either because of the presence of a nuclear stellar cluster (in NGC 3021, NGC 4245, and NGC 5879) or due to a larger galactic distance (for NGC 5347, NGC 5427, and UGC 1395) than otherwise required to trace the $M_\bullet - \sigma_c$ relation at these σ_c regimes. Therefore, we presently do not need to invoke either non-gravitational forces (see Sarzi et al. 2002) or a population of more massive SMBHs (see Greene & Ho 2006) to explain the observed flattening of the $M_\bullet - \sigma_c$ relation at low M_\bullet values.

3.3. The upper end of the $M_\bullet - \sigma_c$ relation

At high σ_c ($> 220 \text{ km s}^{-1}$) our M_\bullet upper limits nicely bracket the $M_\bullet - \sigma_c$ relation (Fig. 5e) and most of them are consistent with its scatter (Fig. 3). In fact, only four objects (15%; NGC 2911, NGC 4552, NGC 4594, and NGC 5077) fall above the $M_\bullet - \sigma_c$ relation by more than its scatter, with the same number of galaxies falling as far below the $M_\bullet - \sigma_c$ relation (NGC 3998, NGC 4278, NGC 6861, and UGC 1841). These outliers do not stand out from the rest of the objects with $\sigma_c > 220 \text{ km s}^{-1}$ for any obvious property such as morphology, nuclear activity or distance. This behavior is suggestive of an actual flattening of the high-mass end of $M_\bullet - \sigma_c$ relation, in particular considering that in the most massive and radio-loud galaxies the ionized-gas velocity dispersion can show a significant excess over a purely gravitational model (e.g., Verdoes Kleijn et al. 2006)⁹.

The flattening at high- σ values is less evident when our upper limits are compared to the shallower $M_\bullet - \sigma_e$ relation of Lauer et al. (2007), but is nonetheless present upon closer inspection. In particular, excluding objects with $\sigma_e < 90 \text{ km s}^{-1}$ where the impact of the stellar potential on our M_\bullet estimates could be more important,

3.78 ± 0.27 and 3.56 ± 0.26 , respectively.

This finding would be in agreement with the predictions of semi-analytic models for the coevolution of SMBHs and galaxies at the highest end of the mass spectrum, whereby galaxies and SMBHs grow mainly via gas-poor, dry mergers (Schawinski et al. 2006). Yet, the behavior of $M_\bullet - \sigma_c$ relation in this regime is still under debate. In particular, the limited number of galaxies with reliable M_\bullet measurement in the range $M_\bullet > 10^9 M_\odot$ are actually consistent with a steepening of the $M_\bullet - \sigma_c$ relation (e.g., Wyithe 2006; Dalla Bontà et al. 2008). Furthermore, the cutoff at $\sigma_c \sim 400 \text{ km s}^{-1}$ of the local velocity dispersion function (Seth et al. 2008) implies either that SMBHs with $M_\bullet > 3 \times 10^9 M_\odot$ are extremely rare or that if they exist their host galaxies should lay considerably above the present $M_\bullet - \sigma_c$ relation. In fact, at these regimes Lauer et al. (2007) argue that the stellar luminosity L is better suited than σ_c to trace M_\bullet . The $M_\bullet - \sigma_c$ relation should steepen at its high- σ_c end if Lauer et al. arguments are correct, since the observed σ_c saturates for the most massive of ellipticals while considering increasingly large values of L .

Although our results suggest a flattening of the $M_\bullet - \sigma_c$ relation, we need to keep in mind that systematic effects related to the measurement of the bulge properties may be significant at the high- σ_c end of the $M_\bullet - \sigma_c$ plane. In particular, the aperture correction for the stellar velocity dispersion may be both more important and more uncertain for the most massive of ellipticals than for smaller elliptical and lenticular galaxies. Indeed, giant ellipticals tend to have shallower central surface brightness profiles than their less massive counterparts, which makes the aperture correction more sensitive to the quality and spatial coverage of the stellar kinematics and to uncertainties on the value of the galaxy effective radius, r_e . Incidentally, measurements of r_e are also generally less accurate for giant ellipticals, due the presence of extended stellar halos. Ideally, rather than σ_c one would like to have a quantity that is more closely connected to the stellar mass, such as the total K -band luminosity, which is also known to relate to M_\bullet (Marconi & Hunt 2003), or a *direct* measurement of σ_e . Obtaining the K -band luminosity of our sample galaxies would require much deeper images than the available 2MASS data, whereas properly measuring σ_e requires integral-field observations, such as those derived in the case of the SAURON survey (Emsellem et al. 2007).

3.4. Summary

Owing to the exquisite spatial resolution of HST and to the concentrated character of the ionized-gas emission in low-luminosity AGNs, we have been able to set tight

factor 2.7, with 68% of our upper limits falling immediately above the $M_{\bullet} - \sigma_c$ relation and without exceeding the expected M_{\bullet} values by more than a factor 4.1.

- That our nebular line-width measurements trace rather well the nuclear gravitational potential, makes large samples of M_{\bullet} upper-limit measurements useful in constraining the frequency of objects with exceedingly low or high values of M_{\bullet} and in probing the black-hole mass budget across the entire Hubble sequence.
- No systematic trends or offsets are observed in this σ_c range as a function of the galaxy Hubble type, or with respect to the presence of a bar. Furthermore, no evidence was found to suggest that the largest or smallest M_{\bullet} upper limit in the σ_c range between 90 and 220 km s⁻¹ are actually bracketing exceptionally high or low values of M_{\bullet} . Thus, galaxies with exceedingly high M_{\bullet} budgets must be very rare.
- For σ_c values below 90 km s⁻¹ half of our M_{\bullet} upper limits systematically exceed the expected M_{\bullet} values by more than a factor 40, consistent with previous work on much smaller samples.

The line-width measurements for such low- σ_c outliers are most likely affected by the stellar contribution to the gravitational potential, either due to the presence of a nuclear stellar cluster or because of a greater distance compared to the other galaxies at the low- σ_c end of the $M_{\bullet} - \sigma_c$ relation, for which our M_{\bullet} upper limits are closer to the expected M_{\bullet} values.

- At the opposite σ_c end of the $M_{\bullet} - \sigma_c$ relation, for values of σ_c above 220 km s⁻¹, our M_{\bullet} upper bounds appear to lie much closer the expected M_{\bullet} in the most massive elliptical galaxies, even falling

below the $M_{\bullet} - \sigma_c$ relation. This flattening is less evident when our upper limits are compared with the shallower $M_{\bullet} - \sigma_e$ relation by Lauer et al. (2007), but is nonetheless present upon closer inspection. In particular, excluding objects with $\sigma_e < 90$ km s⁻¹, we found a systematic flattening in the main trend of our upper limits as the high- σ_e end of the $M_{\bullet} - \sigma_e$ plane is progressively populated.

Although such a flattening of the $M_{\bullet} - \sigma_c$ relations at its high- σ_c end would appear consistent with models for the coevolution of supermassive black holes and galaxies driven by dry mergers, we caution that better and more consistent measurements for either the K -band luminosity or the integrated value of the stellar velocity dispersion σ_e within the bulge effective radius r_e (both better tracers of the bulge mass than σ_c) are needed before systematic effects can be ruled out.

Acknowledgments. We acknowledge the anonymous referee for his/her many comments that improved our manuscript. We are indebted with James Binney, Stéphane Courteau, Sadegh Khochfar, Lorenzo Morelli, Kevin Schawinski, and Massimo Stiavelli for many useful discussions and suggestions. We are also indebted with Jonelle Walsh and her collaborators for sharing with us the results of their work prior to publication. We thank Jairo Méndez Abreu for the GASP2D package which we used for measuring the photometric parameters of some of the sample galaxies. We acknowledge the grant CPDA068415/06 by Padua University, which provided support for this research. AB is grateful to the University of Hertfordshire for its hospitality while this paper was in progress. This research has made use of the Lyon-Meudon Extragalactic Database (LEDA), NASA/IPAC Extragalactic Database (NED), and the Two Micron All Sky Survey (2MASS).

REFERENCES

- Aller, M. C., & Richstone, D. O. 2007, ApJ, 665, 120
 Andredakis, Y. C. & Sanders, R. H. 1994, MNRAS, 267, 283
 Atkinson, J. W., et al. 2005, MNRAS, 359, 504
 Baggett, W. E., Baggett, S. M., & Anderson, K. S. J. 1998, AJ, 116, 1626
 Balcells, M., Morganti, R., Oosterloo, T., Perez-Fournon, I., & Gonzalez-Serrano, J. I. 1995, A&A, 302, 665
 Barth, A. J., Ho, L. C., & Sargent, W. L. W. 2002, AJ, 124, 2607
 Barth A. J., Sarzi M., Rix H.-W., Ho L. C., Filippenko A. V., & Sargent W. L. W., 2001, ApJ, 555, 685
 Barth A. J., Strigari L. E., Bentz M. C., Greene J. E., Ho L. C., 2008, arXiv, 809, arXiv:0809.1066
 Batcheldor, D., et al. 2005, ApJS, 160, 76
 Bender, R., Sogrin, R., & Gebhardt, G. F. 1994, MNRAS, 269, 105
 Bower, G. A., et al. 1998, ApJ, 492, L111
 Braatz, J.A., Wilson, A.S., & Henkel, C. 1994, ApJ, 437, L99
 Cappellari M., & McDermid R. M., 2005, CQGra, 22, 347
 Carollo, C. M., Danziger, I. J., & Buson, L. 1993, MNRAS, 265, 553
 Coccato, L., et al. 2006, MNRAS, 366, 1050
 Corsini, E. M., et al. 1999, A&A, 342, 671
 Côté, P., et al. 2006, ApJS, 165, 57
 Dalla Bontà, E., Ferrarese, L., Corsini, E. M., Miralda-Escudé, J., Coccato, L. & Sarzi, M. 2008, ApJ, accepted
 Davies, R. I., et al. 2006, ApJ, 646, 754
 Davies, R. L., Burstein, D., Dressler, A., Faber, S. M., Lynden-Bell, D., Terlevich, R. J., & Wegner, G. 1987, ApJS, 64, 531

- di Nella, H., Garcia, A. M., Garnier, R., & Paturel, G. 1995, *A&AS*, 113, 151
- Dressel, L., et al. 2007, *STIS Data Handbook*, Version 5.0, (Baltimore: STScI)
- Dumas, G., Mundell, C. G., Emsellem, E., & Nagar, N. M. 2007, *MNRAS*, 379, 1249
- Emsellem, E., et al. 2007, *MNRAS*, 379, 401
- Faber, S. M., & Jackson, R. E. 1976, *ApJ*, 204, 668
- Falcón-Barroso, J., Peletier, R. F., & Balcells, M. 2002, *MNRAS*, 335, 741
- Falcón-Barroso, J., et al. 2006, *MNRAS*, 369, 529
- Ferrarese, L., Ford, H. C., & Jaffe, W. 1996, *ApJ*, 470, 444
- Ferrarese, L., & Merritt, D. 2000, *ApJ*, 539, L9
- Ferrarese, L. 2002, *ApJ*, 578, 90
- Ferrarese, L. & Ford, H. 2005, *Sp. Sci. Rev.*, 116, 523
- Ferrarese, L., et al. 2006, *ApJ*, 644, L21
- Filippenko, A. V., & Halpern, J. P. 1984, *ApJ*, 285, 458
- Filippenko, A. V., & Sargent, W. L. W. 1988, *ApJ*, 324, 134
- Fisher, D. 1997, *AJ*, 113, 950
- Fisher, D., Franx, M., & Illingworth, G. 1995, *ApJ*, 448, 119
- Freedman, W. L., et al. 2001, *ApJ*, 553, 47
- García-Rissmann, A., Vega, L. R., Asari, N. V., Cid Fernandes, R., Schmitt, H., González Delgado, R. M., & Storchi-Bergmann, T. 2005, *MNRAS*, 359, 765
- Gebhardt, K., et al. 2000, *ApJ*, 539, L13
- Gebhardt, K., et al. 2003, *ApJ*, 583, 92
- Graham, A. W., Erwin, P., Caon, N., & Trujillo, I. 2001, *ApJ*, 563, L11
- Graham, A. W. 2008, *ApJ*, 680, 143
- Greene, J. E., & Ho, L. C. 2006, *ApJ*, 641, L21
- Greenhill, L. J., Kondratko, P. T., Lovell, J. E. J., Kuiper, T. B. H., Moran, J. M., Jauncey, D. L., & Baines, G. P. 2003, *ApJ*, 582, L11
- Gu, Q., Melnick, J., Fernandes, R. C., Kunth, D., Terlevich, E., & Terlevich, R. 2006, *MNRAS*, 366, 480
- Jarvis, B. J., Dubath, P., Martinet, L., & Bacon, R. 1988, *A&AS*, 74, 513
- Jørgensen, I., Franx, M., & Kjaergaard, P. 1995, *MNRAS*, 276, 1341
- Haehnelt, M. G., & Kauffmann, G. 2000, *MNRAS*, 318, L35
- Håring, N., & Rix, H.-W. 2004, *ApJ*, 604, L89
- Héraudeau, P. & Simien, F. 1998, *A&AS*, 133, 317
- Héraudeau, P., Simien, F., Maubon, G., & Prugniel, P. 1999, *A&AS*, 136, 509
- Ho, L. C., Filippenko, A. V., & Sargent, W. L. W., 1997, *ApJS*, 112, 315
- Ho, L. C., Filippenko, A. V., Sargent, W. L. W., & Peng, C. Y. 1997, *ApJS*, 112, 391
- Ho, L. C., Rudnick, G., Rix, H.-W., Shields, J. C., McIntosh, D. H., Filippenko, A. V., Sargent, W. L. W., & Eracleous, M. 2000, *ApJ*, 541, 120
- Ho, L. C., Sarzi, M., Rix, H.-W., Shields, J. C., Rudnick, G., Filippenko, A. V., & Barth, A. J. 2002, *PASP*, 114, 137
- Ho, L. C. 2008, *ARA&A*, in press (arXiv:0803.2268)
- Houghton R. C. W., Magorrian J., Sarzi M., Thatte N., Davies R. L., & Krajnović D., 2006, *MNRAS*, 367, 2
- Kassin, S. A., de Jong, R. S., & Pogge, R. W. 2006, *ApJS*, 162, 80
- Kazantzidis, S., et al. 2005, *ApJ*, 623, L67
- Kim Quijano, J., et al. 2007, *STIS Instrument Handbook*, Version 8.0 (Baltimore: STScI)
- Koprolin, W., & Zeilinger, W. W. 2000, *A&AS*, 145, 71
- Kormendy, J. 1988, *ApJ*, 335, 40
- Kormendy, J., & Richstone, D. 1995, *ARA&A*, 33, 581
- Kormendy, J. 2004, in *Coevolution of Black Holes and Galaxies*, McLaughlin, D. E., King, A. R., & Nayakshin, S. 2006, *ApJ*, 650, L37
- Méndez-Abreu, J., Aguerri, J. A. L., Corsini, E. M., & Simonneau, E. 2008, *A&A*, 478, 353
- More, J. J., Garbow, B. S., & Hillstrom, K. E. 1980, *User guide for MINPACK-1*, Report ANL-80-74 Argonne: Argonne National Laboratory)
- Miyoshi, M., Moran, J., Herrnstein, J., Greenhill, L., Nakai, N., Diamond, P., & Inoue, M. 1995, *Nature*, 373, 127
- Nelson, C. H. & Whittle, M. 1995, *ApJS*, 99, 67
- Noel-Storr, J., Baum, S. A., & O’Dea, C. P. 2007, *ApJ*, 663, 71
- Novak, G. S., Faber, S. M., & Dekel, A. 2006, *ApJ*, 637, 96
- Nowak, N., Saglia, R. P., Thomas, J., Bender, R., Pannella, M., Gebhardt, K., & Davies, R. I. 2007, *MNRAS*, 379, 909
- Osterbrock, D. E. 1989, *Astrophysics of Gaseous Nebulae and Active Galactic Nuclei* (Mill Valley: University Science Books)
- Pastorini, G., et al. 2007, *A&A*, 469, 405
- Pizzella, A., Corsini, E. M., Dalla Bontà, E., Sarzi, M., Coccato, L., & Bertola, F. 2005, *ApJ*, 631, 785
- Proctor, R. N. & Sansom, A. E. 2002, *MNRAS*, 333, 517
- Press, W. H., Teukolsky, S. A., Vetterling, W. T., & Flannery, B. P. 1996, *Numerical Recipes in Fortran 77: The Art of Scientific Computing* (Cambridge: Cambridge University Press)
- Rice, M. S., Martini, P., Greene, J. E., Pogge, R. W., Shields, J. C., Mulchaey, J. S., & Regan, M. W. 2006, *ApJ*, 636, 654
- Sarzi, M., Rix, H.-W., Shields, J. C., Rudnick, G., Ho, L. C., McIntosh, D. H., Filippenko, A. V., & Sargent, W. L. W. 2001, *ApJ*, 550, 65
- Sarzi, M., et al. 2002, *ApJ*, 567, 237
- Sarzi M., 2004, in *Coevolution of Black Holes and Galaxies*, ed. L. C. Ho (Cambridge: Cambridge Univ. Press), 1
- Sarzi M., et al., 2006, *MNRAS*, 366, 1151
- Scarlata, C., et al. 2004, *AJ*, 128, 1124
- Shapiro, K. L., Cappellari, M., de Zeeuw, T., McDermid, R. M., Gebhardt, K., van den Bosch, R. C. E., & Statler, T. S. 2006, *MNRAS*, 370, 559
- Schawinski, K., et al. 2006, *Nature*, 442, 888
- Schechter, P. L. 1983, *ApJS*, 52, 425
- Seth, A., Agüeros, M., Lee, D., & Basu-Zych, A. 2008, *ApJ*, 678, 116
- Skrutskie, M. F., et al. 2006, *AJ*, 131, 1163 (2MASS)
- Silk, J., & Rees, M. J. 1998, *A&A*, 331, L1
- Simien, F. & Prugniel, P. 1997a, *A&AS*, 122, 521
- Simien, F. & Prugniel, P. 1997b, *A&AS*, 126, 15
- Simien, F. & Prugniel, P. 1997c, *A&AS*, 126, 519
- Simien, F. & Prugniel, P. 1997c, *A&AS*, 131, 287
- Simien, F. & Prugniel, P. 2002, *A&AS*, 384, 371
- Smith, R. J., Lucey, J. R., Hudson, M. J., Schlegel, D. J., & Davies, R. L. 2000, *MNRAS*, 313, 469
- Terlevich, E., Díaz, A. I., & Terlevich, R. 1990, *MNRAS*, 242, 271
- Tonry, J. L. & Davis, M. 1981, *ApJ*, 246, 666
- Tonry, J. L., Dressler, A., Blakeslee, J. P., Ajhar, E. A., Fletcher, A. B., Luppino, G. A., Metzger, M. R., & Moore, C. B. 2001, *ApJ*, 546, 681
- Tully, R. B. 1988, *Nearby Galaxies Catalog* (Cambridge: Cambridge University Press)
- Tonry, J. L., Blakeslee, J. P., Ajhar, E. A., & Dressler, A. 2000, *ApJ*, 530, 625
- Tremaine, S., et al. 2002, *ApJ*, 574, 740
- Valluri, M., Merritt, D., & Emsellem, E. 2004, *ApJ*, 602, 66
- van den Bosch, F. C. & van der Marel, R. P. 1995, *MNRAS*, 274, 884
- van Dokkum, P. G., 2001, *PASP*, 113, 1420
- van der Marel, R. P. & van den Bosch, F. C. 1998, *AJ*, 116, 2220

- Vittorini, V., Shankar, F., & Cavaliere, A. 2005, MNRAS, 363, 1376
- Wagner, S. J. & Appenzeller, I. 1988, A&A, 197, 75
- Walsh, J. L., Barth A. J., Ho L. C., Filippenko A. V., Rix H.-W., Shields, J. C., Sarzi M., & Sargent W. L. W. 2008, ApJ, submitted.
- Wegner, G., et al. 2003, AJ, 126, 2268
- Wyithe J. S. B., 2006, MNRAS, 365, 1082
- Whitmore, B. C. & Kirshner, R. P. 1981, ApJ, 250, 43
- Whitmore, B. C., Schechter, P. L., & Kirshner, R. P. 1979, ApJ, 234, 68
- Xanthopoulos, E. 1996, MNRAS, 280, 6

Table 1:: PROPERTIES OF THE SAMPLE GALAXIES

sh. T.	Spec. Cl.	D (Mpc)	Ref.	M_B^0 (mag)	τ_e ($''$)	Band	Ref.	σ_c (km s^{-1})	Ref.	Prop.	Apert. ($''$)	(pc)	σ_g (km s^{-1})	M_\bullet ($i = 33^\circ$) (M_\odot)	M_\bullet ($i = 81^\circ$) (M_\odot)	M_\bullet (low,high) (M_\odot)	Ref.
(2)	(3)	(4)	(5)	(6)	(7)	(8)	(9)	(10)	(11)	(12)	(13)	(14)	(15)	(16)	(17)	(18)	(19)
(rs)	H	4.0	1	-21.97	64.1	K	5	71 ± 26	17	8591	0.15×0.1	3×2	60 ± 4	5.4E6	1.4E6		
(rs):	S2*	48.0	2	-20.70	3.4	K	5	99 ± 5	18	9143	0.25×0.2	58×46	96 ± 3	2.5E7	4.8E6		
(s):	...	53.2	2	-20.22	3.5	K	5	201 ± 1	19	8236	0.30×0.2	77×52	183 ± 14	5.6E8	1.3E8		
(s)	...	18.3	2	-19.91	4.0	K	6	118 ± 12	20	8228	0.25×0.2	22×18	79 ± 6	5.0E7	1.3E7		
(s)	L1.9	61.8	2	-22.09	36.9	B	2	340 ± 29	21	8236	0.15×0.1	45×30	335 ± 11	1.8E9	4.3E8		
(s)	...	63.4	2	-21.33	6.5	K	5	259 ± 18	22	8236	0.15×0.1	46×31	248 ± 19	1.3E9	2.9E8		
(s)	...	68.2	2	-21.19	35.8	R	7	208 ± 4	23	8236	0.30×0.2	99×66	206 ± 17	9.2E8	1.9E8		
(s)	H*	16.5	2	-20.56	4.2	H	8	136 ± 20	24	8228	0.25×0.2	20×16	151 ± 9	9.6E7	1.9E7		
(s)	...	70.4	2	-22.17	52.1	B	2	252 ± 12	25	8236	0.30×0.2	102×68	496 ± 44	1.2E9	2.1E8		
(s)	S1/S2*	51.3	2	-20.75	17.5	I	9	138 ± 20	26	9143	0.25×0.2	62×50	159 ± 5	5.4E8	1.4E8		
(s)	L1.9	19.4	3	-20.09	33.7	B	2	207 ± 7	27	7403	0.25×0.2	23×19	226 ± 5	3.6E8	9.4E7		
(s)	S2	51.6	2	-20.86	10.8	V	9	186 ± 20	26	9143	0.25×0.2	62×50	176 ± 1	5.3E8	1.2E8		
(s)	...	80.6	2	-21.24	19.5	K	5	249 ± 1	19	7354	0.15×0.1	59×39	276 ± 18	7.1E8	3.0E8		
(s)	S2	60.1	2	-21.49	0.3	V	9	193 ± 31	17	9143	0.25×0.2	73×58	97 ± 1	2.9E8	1.0E8		
(s)	L2	52.1	2	-22.58	139.1	V	10	241 ± 41	24	9106	0.30×0.2	76×50	167 ± 4	4.6E8	9.4E7		
(s)	S2*	31.2	2	-20.62	14.9	V	9	219 ± 25	26	8610	0.25×0.2	38×30	242 ± 4	6.2E8	3.2E7		
(s)	...	38.4	2	-20.09	8.9	V	10	168 ± 12	28	9068	0.25×0.2	46×37	137 ± 8	3.8E8	1.3E8		
(s)	S2	25.0	2	-19.97	2.6	K	14	127 ± 11	26	9143	0.25×0.2	30×24	27 ± 1	7.1E6	2.1E6		
(s)	...	77.5	2	-21.36	20.3	B	15	236 ± 14	29	8236	0.30×0.2	113×75	201 ± 8	2.5E8	1.1E8		
(s)	S2/T2:	13.4	2	-18.81	15.2	V	10	89 ± 8	30	8607	0.30×0.2	19×13	69 ± 4	1.1E7	1.6E6		
(s)	H	19.9	2	-19.90	78 ± 5	20	8228	0.25×0.2	24×19	43 ± 4	1.6E7	1.6E7	4.4E7(0.8,7.9)	57
(s)	L1.9	7.5	3	-17.76	17.3	V	10	199 ± 5	27	7361	0.25×0.2	9×7	209 ± 6	8.2E7	1.7E7	9.0E7(2.1,15.8)	58
(s)	H	11.2	2	-21.14	5.7	V	10	102 ± 13	31	8228	0.30×0.2	16×11	74 ± 4	2.4E7	6.4E6		
(s)	L2	46.6	2	-21.09	7.0	K	14	238 ± 17	32	7354	0.15×0.1	34×23	400 ± 38	2.6E9	6.6E8		
(s)	H	21.1	2	-20.03	0.8	V	10	106 ± 21	31	8228	0.25×0.2	26×20	80 ± 4	2.4E7	1.4E6		
(s)	...	23.9	2	-19.37	2.9	K	16	61 ± 27	33	8228	0.25×0.2	29×23	69 ± 4	4.0E7	9.8E6		
(s)	S1.5	3.9	3	-20.57	66.2	V	10	152 ± 4	34	7351	0.15×0.1	3×2	192 ± 1	4.1E7	8.4E6	9.0E7(2.1,15.8)	59
(s)	...	35.2	3	-20.79	22.8	B	2	226 ± 13	35	9163	0.30×0.2	51×34	192 ± 6	2.2E8	3.3E7		
(s)	S2*	35.9	2	-20.19	4.2	K	9	134 ± 8	18	9143	0.25×0.2	43×35	52 ± 1	3.4E7	8.5E6		
(s)	S1.5	19.6	2	-20.28	1.3	V	10	138 ± 14	26	7403	0.25×0.2	24×19	117 ± 3	6.3E7	1.2E7	1.5E7(1.0,2.0)	60
(s)	T2:	20.9	3	-19.53	15.6	V	10	205 ± 18	36	7403	0.25×0.2	25×20	138 ± 8	2.5E8	4.8E7	2.1E8(1.6,2.6)	61
(s)	H	15.6	2	-20.01	5.4	V	10	113 ± 29	17	8228	0.30×0.2	23×15	46 ± 1	1.5E7	5.0E6	< 4.7E7	62
(s)	L2	10.0	4	-19.74	13.1	V	10	104 ± 16	37	7361	0.25×0.2	12×10	45 ± 2	6.4E6	1.9E6		
(s)	H	10.4	3	-20.28	56.4	V	10	114 ± 4	34	7361	0.25×0.2	13×10	97 ± 4	4.8E7	1.5E7		
(s)	S2*	54.2	2	-21.03	8.7	K	5	182 ± 28	17	8055	0.25×0.2	66×52	91 ± 3	2.5E8	9.4E7		
(s)	T2/S2	10.1	4	-20.88	51.9	V	10	108 ± 8	31	8607	0.30×0.2	15×10	79 ± 2	1.5E7	6.8E6		
(s)	L1.9	23.2	2	-20.37	28.4	V	10	104 ± 27	17	8228	0.25×0.2	28×22	147 ± 11	3.1E7	2.6E7		
(s)	T2	13.3	2	-20.10	13.4	H	8	118 ± 5	31	8607	0.30×0.2	19×13	80 ± 4	3.9E7	1.0E7		
(s)	...	49.6	2	-20.69	5.5	K	5	228 ± 19	32	8236	0.30×0.2	72×48	166 ± 10	4.2E8	1.0E8		
(s)	...	90.6	2	-21.27	17.7	B	2	240 ± 15	38	8236	0.30×0.2	132×88	188 ± 7	6.4E8	1.2E8		
(s)	T2	16.5	2	-20.71	32.0	V	10	140 ± 1	20	8228	0.30×0.2	24×16	103 ± 6	4.5E7	1.2E7		
(s)	S1.9	17.0	2	-19.47	78 ± 2	39	7361	0.25×0.2	21×16	49 ± 2	1.7E7	5.2E6		
(s)	T2:	16.4	2	-20.81	64.4	V	10	131 ± 19	39	7361	0.25×0.2	20×16	103 ± 3	6.7E7	1.8E7		
(s)	L1.9	14.1	3	-19.26	17.6	V	10	302 ± 8	40	7354	0.15×0.1	10×7	426 ± 11	3.5E8	5.0E7	2.7E8(0.3,4.7)	63
(s)	L1.9	20.4	2	-20.06	19.9	V	10	167 ± 5	40	7403	0.25×0.2	25×20	205 ± 5	1.9E8	3.6E7		
(s)	H	18.2	2	-19.54	9.1	K	5	95 ± 5	20	8228	0.25×0.2	22×18	36 ± 2	4.4E6	1.0E6	< 2.0E7	64
(s)	H	12.7	2	-20.00	2.4	V	10	93 ± 4	20	8228	0.25×0.2	15×12	50 ± 5	1.3E7	3.4E6		
(s)	L1.9	15.9	3	-19.11	0.9	V	10	230 ± 6	41	7361	0.25×0.2	19×15	211 ± 3	2.0E8	4.0E7		
(s)	T2	13.7	3	-18.29	0.9	V	10	97 ± 3	26	8607	0.30×0.2	20×13	69 ± 9	2.6E6	3.4E5		
(s)	L1.9	15.1	3	-19.29	14.7	V	10	166 ± 3	27	7361	0.25×0.2	18×15	139 ± 3	1.3E8	3.9E7	< 5.2E7	58
(s)	H	3.4	2	-16.28	22.4	V	10	74 ± 3	20	8228	0.25×0.2	4×3	59 ± 5	2.8E6	4.0E5		
(s)	H	15.6	2	-18.96	5.7	V	10	89 ± 10	42	7361	0.25×0.2	19×15	117 ± 24	5.0E7	5.6E6		
(s)	S1.9	7.3	3	-20.78	332.4	V	10	99 ± 9	31	8228	0.25×0.2	9×7	175 ± 3	4.8E7	9.1E6	3.9E7(3.6,4.2)	65
(s)	L2	31.6	3	-21.14	36.1	B	2	288 ± 14	38	8236	0.15×0.1	23×15	188 ± 8	3.8E8	9.3E7	5.4E8(4.2,6.6)	67
(s)	L1.9	16.1	3	-20.06	34.4	B	2	251 ± 8	27	7403	0.25×0.2	19×16	333 ± 8	1.8E8	5.2E7		
(s)	L2	16.6	2	-19.93	21.0	V	10	115 ± 4	27	7361	0.25×0.2	20×16	56 ± 5	1.7E7	4.4E6		
(s)	T2	15.2	4	-20.93	20.7	V	10	90 ± 4	27	7361	0.25×0.2	18×15	65 ± 1	7.4E6	3.4E6		
(s)	...	63.3	2	-20.67	15.0	K	2	289 ± 6	43	8236	0.30×0.2	92 ± 61	171 ± 8	5.5E8	1.3E8	< 6.0E8	43
(s)	L2	18.4	3	-21.31	50.9	B	2	291 ± 7	27	7124	0.25×0.2	22×18	396 ± 14	1.4E9	4.7E8	1.5E9(0.7, 1.8)	66
(s)	T2	19.5	2	-20.48	28.0	V	10	185 ± 8	29	8607	0.30×0.2	28×19	134 ± 5	1.7E8	3.4E7		
(s)	T2/H:	14.8	2	-19.23	24.0	V	10	149 ± 7	29	7361	0.25×0.2	18×14	98 ± 4	4.8E7	1.6E7	< 7.5E6	68
(s)	L1.9	30.3	2	-21.66	10.8	V	10	120 ± 16	44	7361	0.25×0.2	37×29	138 ± 3	2.4E8	6.5E7		

Table 1 – Continued

Obs. T.	Spec. Cl.	D (Mpc)	Ref.	M_B^0 (mag)	r_e ($''$)	Band	Ref.	σ_c (km s^{-1})	Ref.	Prop.	Apert. ($''$)	Apert. (pc)	σ_g (km s^{-1})	M_\bullet ($i = 33^\circ$) (M_\odot)	M_\bullet ($i = 81^\circ$) (M_\odot)	M_\bullet (low,high) (M_\odot)	Ref.
(2)	(3)	(4)	(5)	(6)	(7)	(8)	(9)	(10)	(11)	(12)	(13)	(14)	(15)	(16)	(17)	(18)	(19)
r)	T2:	16.1	3	-19.83	16.7	V	10	179 ± 13	23	7361	0.25×0.2	19×16	216 ± 9	2.4E8	3.0E7	7.0E7(5.7,8.3)	58
?	S2	22.3	2	-20.44	24.4	V	10	154 ± 9	45	7361	0.25×0.2	27×22	110 ± 2	7.6E7	1.9E7		
pec	L2	15.9	3	-21.51	94.9	B	2	349 ± 8	23	8666	0.25×0.2	19×15	630 ± 14	2.9E9	8.8E8	3.8E9(2.8,4.8)	69
)	S2	34.6	2	-22.84	6.0	V	10	152 ± 17	31	7361	0.25×0.2	42×33	99 ± 1	8.0E7	1.5E7		
Bb(rs)	S2*	50.4	2	-21.23	1.9	K	5	156 ± 7	18	9143	0.25×0.2	61×49	54 ± 3	3.6E7	7.3E6		
)	H	16.9	3	-20.61	19.7	V	10	208 ± 3	46	9163	0.25×0.2	20×16	320 ± 11	3.2E8	6.1E7		
)	L2	19.2	3	-20.63	35.2	V	10	153 ± 14	44	7361	0.25×0.2	23×19	77 ± 2	3.8E7	9.6E6		
)	T2:	15.4	3	-20.36	29.3	B	2	254 ± 11	29	8472	0.25×0.2	19×15	476 ± 18	1.9E9	6.9E8		
(rs)	S1.9/L1.9	24.6	2	-21.66	17.0	V	10	123 ± 16	31	7403	0.25×0.2	30×24	231 ± 2	2.3E8	4.3E7		
sp	L2	9.8	3	-21.57	50.9	V	10	226 ± 6	38	7354	0.15×0.1	7×5	489 ± 20	8.6E8	2.4E8	1.0E9(0.3,1.7)	70
)	L2::	29.3	2	-20.83	17.4	V	10	148 ± 14	47	7361	0.25×0.2	35×28	162 ± 11	2.0E8	4.0E7	8.0E7(4.0,12.0)	58
)	L1.9	14.7	3	-20.40	88.5	B	2	178 ± 9	48	8472	0.25×0.2	18×14	254 ± 13	6.8E8	2.5E8		
)	S2	17.6	2	-19.99	29.4	V	10	129 ± 9	28	7361	0.25×0.2	21×17	92 ± 2	8.9E7	4.3E7		
b(r)	L2	5.2	3	-19.83	45.2	V	10	106 ± 3	27	8591	0.15×0.1	4×2	90 ± 5	1.4E7	3.3E6		
)	H	13.4	2	-18.51	15.4	R	11	111 ± 2	39	7361	0.25×0.2	16×13	95 ± 10	3.9E7	3.3E6		
b(rs)	T2	7.5	3	-20.55	5.0	V	10	115 ± 13	31	8607	0.30×0.2	11×7	99 ± 4	4.2E7	1.8E7		
(rs)	L1.9	15.7	2	-20.79	5.8	V	10	215 ± 8	20	8228	0.25×0.2	19×15	204 ± 3	3.4E8	1.2E8		
)	L1.9	41.9	2	-20.90	22.8	B	2	239 ± 11	35	7354	0.15×0.1	30×20	397 ± 13	2.0E9	4.4E8	6.8E8(4.0,11.6)	71
)	...	67.0	2	-21.32	48.1	K	5	194 ± 5	49	8236	0.30×0.2	97×65	153 ± 7	5.1E8	7.7E7		
)	S2	8.5	2	-20.99	47.7	V	10	76 ± 10	26	9147	0.25×0.2	10×8	36 ± 2	2.3E6	4.3E5		
(rs)	H	19.2	2	-20.78	0.6	R	16	128 ± 12	50	8228	0.25×0.2	23×19	45 ± 4	5.1E6	9.0E5		
)	S1.9*	95.7	2	-20.97	20.7	J	12	183 ± 26	26	8055	0.25×0.2	116×93	197 ± 6	7.0E8	1.3E8		
)	S2*	37.0	2	-18.72	8.7	K	5	148 ± 14	26	9143	0.25×0.2	45×36	61 ± 3	5.9E7	1.3E7		
ab(rs)	S2*	34.6	2	-19.59	20.5	V	10	70 ± 13	26	9143	0.25×0.2	42×33	53 ± 3	4.6E7	6.5E6		
pec	S2*	38.9	2	-21.22	29.7	V	10	70 ± 12	26	9143	0.25×0.2	47×38	78 ± 1	8.1E7	2.0E7		
)	...	70.0	2	-21.34	18.5	B	2	292 ± 28	29	8236	0.30×0.2	102×68	278 ± 21	1.3E9	2.6E8		
)	S2*	18.6	2	-21.11	2.6	H	8	97 ± 1	51	9143	0.25×0.2	22×18	95 ± 3	4.7E7	3.1E6		
)	S2*	58.5	2	-20.46	7.1	K	5	148 ± 2	26	9143	0.25×0.2	71×57	67 ± 2	2.2E8	5.1E7		
)	S2*	40.3	2	-21.37	56.0	V	10	210 ± 44	52	8123	0.15×0.1	29×19	121 ± 7	2.4E8	6.2E7		
)	T2/L2	11.4	2	-18.88	3.0	B	13	59 ± 9	13	8607	0.30×0.2	17×11	73 ± 4	8.5E6	2.4E6		
)	S2*	15.2	2	-20.71	6.0	K	6	94 ± 5	18	9143	0.25×0.2	18×15	75 ± 5	2.4E7	9.4E6		
)	L2	39.1	2	-20.50	2.1	K	5	230 ± 6	27	7354	0.15×0.1	28×19	168 ± 19	4.3E8	1.3E8		
(rs):	...	28.1	3	-20.32	14.9	K	5	419 ± 15	53	9163	0.30×0.2	41×27	623 ± 61	1.5E9	3.6E8		
(rs)	S2	17.1	2	-20.45	5.4	V	10	104 ± 11	24	8228	0.25×0.2	21×17	72 ± 1	1.4E7	5.9E6		
)	...	61.7	2	-21.26	34.7	J	12	239 ± 23	54	8236	0.15×0.1	45×30	235 ± 14	1.2E9	3.1E8	3.7E8(2.2,6.3)	72
)	T2	13.1	3	-21.21	48.6	V	10	126 ± 4	34	8228	0.25×0.2	16×13	204 ± 26	1.7E8	7.4E7		
)	L2::	40.8	2	-20.99	38.7	B	2	253 ± 11	38	8236	0.30×0.2	59×40	279 ± 16	8.7E8	1.9E8		
)	S2*	63.5	2	-20.34	9.4	K	5	122 ± 17	26	9143	0.25×0.2	77×62	112 ± 3	4.8E8	1.9E8		
)	S2*	64.2	2	-20.47	37.0	J	9	116 ± 15	26	9143	0.25×0.2	78×62	76 ± 1	8.9E7	3.9E7		
30+(rs):	S1.9*	65.2	2	-20.21	2.4	K	5	70 ± 6	18	9143	0.25×0.2	79×63	24 ± 3	1.4E7	3.8E6		
)	...	80.3	2	-21.28	348 ± 29	55	8236	0.30×0.2	117×78	330 ± 26	4.9E8	2.0E8		
)	...	94.5	2	-20.70	10.9	B	2	205 ± 38	55	8236	0.30×0.2	137×92	318 ± 14	3.0E9	3.9E8		
)	...	64.4	2	-20.19	2.7	K	5	281 ± 19	55	8236	0.15×0.1	47×31	426 ± 21	2.5E9	2.3E8		

NOTES. — Col.(1): Galaxy name. Col.(2): Morphological type from RC3. Col.(3): Nuclear spectral class from Ho, Filippenko, & Sargent (1997), where H = H II nucleus, L = LINER, S = Seyfert, T = transition object (LINER/HII), 1 = type 1, 2 = type 2, and a fractional number between 1 and 2 denotes various intermediate types; uncertain and highly uncertain classifications are followed by a single and double colon, respectively. The nuclear spectral class of galaxies marked with * is from NASA/IPAC Extragalactic Database (NED). Col.(4): Distance. Col.(5): Reference for col. 4. All the distances were taken from literature (see attached list), except those we obtained from V_{3K} , the weighted mean recessional velocity corrected to the reference frame of the microwave background radiation given in RC3. These were derived as V_{3K}/H_0 with $H_0 = 75 \text{ km s}^{-1} \text{ Mpc}^{-1}$. Col.(6): Absolute corrected B magnitude derived from B_T^0 (RC3) with the adopted distance. Col.(7): Effective radius of the spheroidal component. Col.(8): Band in which the effective radius were measured. Col.(9): Reference for col.(7). All the effective radii were taken from literature (see attached list), except for those we measured by a photometric decomposition of the K -band images available in the 2MASS science archive Skrutskie et al. (2006). Col.(10): Central velocity dispersion of the stellar component within $r_e/8$. Col.(11): Reference for the measured stellar velocity dispersion and corresponding size of the central aperture from which we calculated the value given in col.(10) by following Jørgensen et al. (1995). We did not apply any aperture correction to the measured stellar velocity dispersions of NGC 2748, NGC 3982, and UGC 1841, because no information about the size of the aperture was available. Col.(12): HST proposal number under which was obtained the STIS/G750M spectrum from which we measured the central velocity dispersion of the ionized gas. Col.(13): Size of the central aperture where we measured the velocity dispersion of the ionized gas. Col.(14): Physical size of the central aperture where we measured the velocity dispersion of the ionized gas. Col.(15): Central velocity dispersion of the ionized-gas component within the aperture in Col. (13). This is the intrinsic velocity dispersion obtained from the observed one by subtracting the instrumental velocity dispersion. Col.(16): M_\bullet upper limit for a Keplerian disk model assuming $i = 33^\circ$. Col.(17): M_\bullet upper limit for $i = 81^\circ$. Col.(18): Mass (and confidence interval) of the SMBH derived from modeling based on the resolved kinematics. The M_\bullet of NGC 3227 and NGC 4258 were obtained by studying the dynamics of stars and water masers, respectively. The ionized-gas dynamics was used for all the remaining galaxies. Col.(19): Reference for col.(18).

REFERENCES. — (1) Tully (1988); (2) de Vaucouleurs et al. (1991); (3) Tonry et al. (2001); (4) Freedman et al. (2001); (5) Skrutskie et al. (2006); (6) Kassin et al. (2006); (7) de Souza et al. (2004); (8) Laurikainen et al. (2004); (9) Xanthopoulos (1996); (10) Baggett et al. (1998); (11) Andredakis & Sanders (1994); (12) Marconi & Hunt (2003); (13) Falcón-Barroso et al. (2002); (14) Laurikainen et al. (2005); (15) Fisher et al. (1995); (16) Scarlata et al. (2004); (17) Terlevich et al. (1990); (18) Garcia-Rissmann et al. (2005); (19) Wegner et al. (2003); (20) Batcheldor et al. (2005); (21) Davies et al. (1987); (22) Simien & Prugniel (1997a); (23) Bernardi et al. (2002); (24) Schechter (1983); (25) Bonfanti et al. (1995); (26) Nelson & Whittle (1995); (27) Barth et al. (2002); (28) Corsini et al. (1999); (29) Simien & Prugniel (1997b); (30) Simien & Prugniel (1997c); (31) Héraudeau & Simien (1998); (32) di Nella et al. (1995); (33) Héraudeau et al. (1999); (34) Vega Beltrán et al. (2001); (35) Carollo et al. (1993); (36) Simien & Prugniel (1998); (37) Whitmore et al. (1979); (38) Smith et al. (2000); (39) Sarzi et al. (2002); (40) Fisher (1997); (41) Simien & Prugniel (2002); (42) Falcón-Barroso et al. (2006); (43) Verdoes Kleijn et al. (2002); (44) Whitmore & Kirshner (1981); (45) Jarvis et al. (1988); (46) Proctor & Sansom (2002); (47) Bettoni & Galletta (1997); (48) Bender et al. (1994); (49) Noel-Storr et al. (2007); (50) Dumas et al. (2007); (51) Gu et al. (2006); (52) Wagner & Appenzeller (1988); (54) van den Bosch & van der Marel (1995); (55) Balcells et al. (1995); (55) Tonry & Davis (1981); (57) Atkinson et al. (2005); (58) Sarzi et al. (2001); (59) Devereux et al. (2003); (60) Davies et al. (2006); (61) Barth et al. (2001); (62) Pastorini et al. (2007); (63) de Francesco et al. (2006); (64) Marconi et al. (2003); (65) Miyoshi et al. (1995); (67) Ferrarese et al. (1996); (68) Coccato et al. (2006); (69) Macchetto et al. (1997); (70) Kormendy (1988); (71) de Francesco et al. (2008); (72) van der Marel & van den Bosch (1998); (66) Bower et al. (1998); (53) Koprolin & Zeilinger (2000).

TABLE 2
 PROPERTIES OF THE GALAXIES REJECTED FROM THE MAIN SAMPLE

Galaxy	Morp. T. (RC3)	Prop.	Rej.
IC 5096	Sbc sp	9046	ns
NGC 0134	SABbc(s)	8228	ns
NGC 0157	SABbc(rs)	8228	ns
NGC 0255	SABbc(rs)	8228	ns
NGC 0278	SABb(rs)	7361	s
NGC 0520	pec	8669	i
NGC 1097	SBb(s)	9782	ds
NGC 1255	SABbc(rs)	8228	n
NGC 1300	SBbc(rs)	8228	p
NGC 1832	SBbc(r)	8228	ns
NGC 2623	pec	8669	i
NGC 2654	SBab sp:	9046	s
NGC 2892	E ⁺ pec:	8236	s
NGC 2976	SAc pec	8591	s
NGC 3003	Sbc?	8228	s
NGC 3049	SBab(rs)	7513	s
NGC 3067	SABab(s)	8596	f
NGC 3162	SABbc(rs)	8228	r
NGC 3254	SAbc(s)	8228	n
NGC 3256	pec	8669	i
NGC 3259	SABbc(rs)	8228	s
NGC 3379	E1	8589	f
NGC 3403	SAbc:	8228	ns
NGC 3489	SAB0 ⁺ (rs)	7361	p
NGC 3516	(R)SB0(s)	8055	d
NGC 3521	SABbc(rs)	8228	ns
NGC 3684	SAbc(rs)	8228	ns
NGC 3686	SBbc(s)	8228	s
NGC 3705	SABab(r)	8607	n
NGC 3756	SABbc(rs)	8228	ns
NGC 3887	SBbc(r)	8228	s
NGC 3917	SAc d:	8607	ns
NGC 3921	(R')SA0/a(rs) pec	8669	i
NGC 3949	SAbc(s)	8228	ns
NGC 3972	SAbc(s)	8228	ns
NGC 4030	SAbc(s)	8228	r
NGC 4038	SBm(s) pec	8669	is
NGC 4039	SBm(s) pec	8669	is
NGC 4051	SABbc(rs)	8228	r
NGC 4100	(R')SAbc(rs)	8228	s
NGC 4138	SA0 ⁺ (rs)	1039	n
NGC 4303	SABbc(rs)	8228	p
NGC 4343	SAb(rs)	9068	s
NGC 4380	SAb(rs):?	7361	n
NGC 4389	SBbc(rs)	8228	ns
NGC 4414	SAc(rc)?	8607	n
NGC 4420	SBbc(r):	8228	s
NGC 4527	SABbc(s)	8607/8228	fn
NGC 4536	SABbc(rs)	8228	r
NGC 4569	SABab(rs)	8607	r
NGC 4676A	S0 pec ? (Irr)	8669	s
NGC 4696	E ⁺ 1 pec	8690	n
NGC 5054	SAbc(s)	8228	s
NGC 5055	SAbc(rs)	7361/8228	n
NGC 5135	SBab(s)	9143	r
NGC 5141	S0	8236	s
NGC 5247	SAbc(s)	8228	ns
NGC 5364	SAbc(rs) pec	8228	n

Upper limits on the masses of 105 Black Holes

NOTES. — Col.(1): Galaxy name. Col.(2): Morphological type from RC3. Col.(3): HST proposal number under which was obtained the STIS/G750M spectrum. Col.(4): Reason of rejection, where d = problem in deblending the emission lines, i = interacting galaxy, f = irregular or strongly asymmetric radial profile of the flux of the [N II] emission line, n = faint or absent emission lines, p = double-peaked emission lines, r = unsuccessful two-dimensional rectification of the spectrum, s = no stellar velocity dispersion available in literature.